Raman generation of coherent phonons of anatase and rutile TiO_2 photoexcited at fundamental absorption edges

Kunie Ishioka*
Nano Characterization Unit, National Institute for Materials Science, Tsukuba, 305-0047, Japan

Hrvoje Petek
Department of Physics and Astronomy, University of Pittsburgh, Pittsburgh, Pennsylvania 15260, USA
(Received 9 May 2012; revised manuscript received 27 August 2012; published 5 November 2012)

Ultrafast phonon dynamics in anatase and rutile TiO_2 single crystals are investigated using 400 nm near ultraviolet light pulses, whose wavelength corresponds to the fundamental absorption edges of both polymorphs. Raman-active phonon modes are observed as coherent modulations in THz frequency range of the reflected light intensity. Coherent amplitudes vary as the crystals are rotated with respect to the pump and probe polarizations, depending on the symmetry of the phonon modes. The polarization dependence is quantitatively reproduced by assuming that both the generation and detection are dominated by the Raman scattering process. No evident resonance enhancement is observed in the coherent amplitudes as we vary the excitation light wavelength around the fundamental absorption edges. These results indicate that the creation of coherent bulk phonons by photodoped carriers is negligible compared with the competing Raman process at the fundamental band gap excitation.

DOI: 10.1103/PhysRevB.86.205201 PACS number(s): 78.47.jg, 63.20.kd, 78.30.Hv

I. INTRODUCTION

Titanium dioxide (TiO_2) is a key optoelectronic material with wide applications ranging from photocatalytic coatings to photovoltaic cells.[1–3] Among the different crystalline structures of TiO_2, rutile [Fig. 1(b)] is the most thermodynamically stable phase, whereas anatase [Fig. 1(a)] is stable in nanocrystalline form at relatively low temperatures.[4] Crystalline lattice properties of single crystal rutile[5,6] and anatase[7–9] have been investigated by means of Raman spectroscopy. The frequencies and linewidths of the Raman phonon modes have been widely used to evaluate the nanocrystalline structure and size.[4,10–13]

There has been a large uncertainty over the band gap energies for both rutile and anatase reported by optical measurements[14–19] and calculations.[20–23] Most studies agreed, however, that the optical absorption edges correspond to an indirect band gap, whereas a symmetry-forbidden direct gap lies close in energy. The optical absorption studies also suggested the opposite nature of exciton states (self-trapped or free) in anatase and rutile.[15,17,18,24] For rutile, resonant one- and two-photon Raman measurements demonstrated the strong exciton-phonon interaction by observing a sharp resonance in phonon scattering efficiencies.[24,25] For anatase, however, no resonant Raman study has been reported at the fundamental absorption edge.

Electron-phonon interaction plays a crucial role in the carrier transport in TiO_2 through phonon-assisted polaron hopping[21,26–28] as well as through scattering of carriers by optical phonons.[29] A THz spectroscopy study on a rutile single crystal found that charge transport is limited by anisotropic electron-phonon coupling on a sub-ps time scale and can be described by Feynman polaron theory.[27] For anatase, time-resolved luminescence studies revealed slow (sub-μs) energy relaxation and recombination of self-trapped excitons.[30,31] For faster, electron-phonon energy transfer, a rough estimation of the time scale (sub-ps) was given by first-principle calculations.[32] In nanocrystal TiO_2 powders, carrier dynamics are dominated by the trapping of electrons and holes at surface defects and deeper traps.[33–37] Still, the transport properties and the underlying electron-phonon coupling in the anatase single crystal and nanocrystal are poorly understood.

Observation of coherent phonons can also reveal sub-ps electron-phonon interaction in crystals. Under nonresonant photoexcitation, the coherent phonons can be driven by the electric field of ultrashort laser pulses via the impulsive stimulated Raman scattering (ISRS).[38] A time-resolved spectroscopic study on rutile (110) single crystal surface observed only one of the four Raman-active fundamental phonon modes as a coherent modulation of reflectivity at 18.4 THz.[39] The observed A_{1g} phonon exhibited a sine-like initial phase, as was expected for the ISRS generation. In addition, seven surface phonon modes were observed at frequencies ranging from 5.4 to 24.5 THz by surface second harmonic generation (SSHG) detection on the same sample. All but one surface phonon modes corresponded to the infrared-active but Raman-inactive phonon modes in the bulk. Three of them exhibited initial phase varying between sine-like and cosine-like depending on the pump polarization, whereas the others were sine-like oscillations. The cosine-like oscillations were attributed to the transient depletion field screening (TDFS) mechanism via excitation of a photoinduced surface current.[40] For rutile (110) surface sensitized with quantum dots, ultrafast interfacial charge injection induced coherent soft surface phonon mode of TiO_2 at 2.9 THz,[41] which had no counterpart among the surface phonon modes observed for the nonsensitized surface.[39] By contrast, there has been no report on coherent surface or bulk phonon excitation for anatase single crystals. An optical Kerr effect study on nanoporous TiO_2 films reported a modulation at 4.3 THz, which corresponds to the lowest-frequency Raman mode of anatase,[42] whereas the other five Raman-active phonon modes at higher frequencies were not observed, presumably because of the limited bandwidth of the excitation pulse.

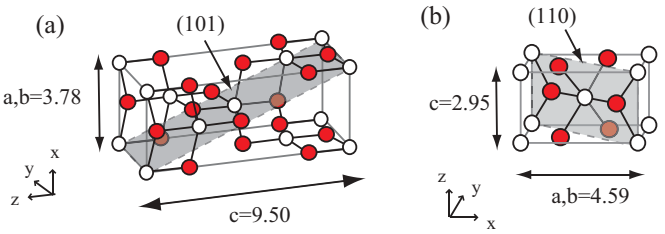

FIG. 1. (Color online) Tetragonal conventional cell of anatase (a) and simple tetragonal unit cell of rutile (b). Oxygen and titanium atoms are colored red and white. Anatase (101) and rutile (110) surface planes are painted gray. x,y,z axes correspond to the [100], [010], [001] directions. Lattice constants are indicated in Å.

The previous coherent phonon studies[39,41,42] employed near infrared or visible light, whose photon energy was insufficient to excite interband transition in TiO_2. In the present study, we examine the bulk phonon dynamics in anatase and rutile single crystals by transient reflectivity measurements with near ultraviolet (NUV) light. The photon energy is close to the fundamental absorption edges at 3.0 and 3.2 eV for rutile and anatase.[15,18,21,22] We observe all the Raman-active bulk phonon modes of anatase as coherent modulations of the reflectivity R with amplitudes $\Delta R/R \leqslant 10^{-7}$. For rutile, only two of the four Raman-active modes are observed. Generation mechanisms of the coherent phonons of both single crystals are investigated by varying the pump polarization angles. Our quantitative analysis of the polarization dependence demonstrates that all the coherent phonons are generated via the ISRS process. At the present photoexcitation condition, the electron-phonon interaction is too weak to cause evident resonant enhancement in the generation of coherent phonons.

II. EXPERIMENT

The investigated samples are a (101)-oriented natural anatase and a (110)-oriented synthetic rutile TiO_2 single crystals purchased from SurfaceNet. The crystalline structures and the surface planes are illustrated in Fig. 1. The samples are investigated under ambient conditions as received.

Pump-probe reflectivity measurements are performed using 400 nm (3.1 eV) light pulses of ~10 fs duration. Linearly polarized pump and probe beams are incident on the sample in a near back-reflection configuration with angles of 15° and 7° from the surface normal. Pump pulse density is ~100 μJ/cm^2 on the sample surface, whereas the probe pulse density is one order of magnitude lower. Photoexcited carrier density is roughly estimated to be ~10^{16} cm^3 for rutile and lower by one to two orders of magnitude for anatase.[18] Pump-induced change in the anisotropic reflectivity ($\Delta R_{\rm eo} = \Delta R_H - \Delta R_V$) is measured in an "electro-optic (EO)" configuration by detecting the difference between the vertically and horizontally polarized components of the reflected probe light. For polarization-dependence measurements, we maintain the pump and probe polarization angles fixed at 0° and 45° from vertical, and rotate the samples around the surface normal axis (approximately parallel to the direction of laser incidence), as illustrated in the inset of Figs. 2(b) and 4(b). Transient reflectivity signal is accumulated and averaged with a 12-bit digital oscilloscope while time delay between pump and probe pulses is scanned repetitively at a 20 Hz rate.

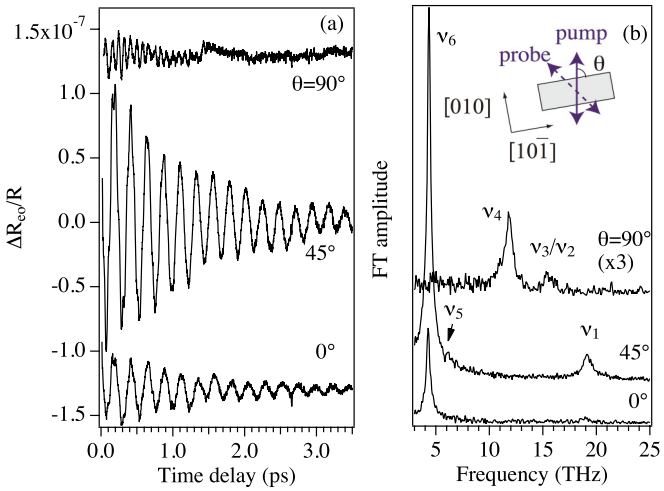

FIG. 2. (Color online) (a) Oscillatory parts of anisotropic reflectivity changes and (b) their FT spectra from anatase (101) surface for different pump polarization angles θ. Traces are offset for clarity. Inset in (b) shows the polarization of pump and probe beams with respect to the crystalline axes. The sample is rotated while the polarizations of pump and probe beams are fixed in vertical and 45° from vertical orientations.

Separate Raman scattering measurements are performed with 532 nm (2.3 eV) excitation light in backscattering geometry. The instrumental wave number resolution is 0.7 cm^{-1}.

III. RESULTS AND DISCUSSION

Figure 2(a) shows the oscillatory part of the pump-induced anisotropic change in the reflectivity $\Delta R_{\rm eo}/R$ from anatase (101) surface. The reflectivity is periodically modulated with amplitudes of 10^{-7} or smaller at frequencies dependent on the orientation of the crystalline axes with respect to the pump and probe polarization directions. Fourier-transformed (FT) spectra in Fig. 2(b) show phonon peaks at 4.4, 5.9, and 19.1 THz when the pump polarization angle θ is 0° or 45° from the [10$\bar{1}$] crystalline axis, and those at 11.8 and 15.2 THz for $\theta = 90°$. The frequencies and dephasing rates of the coherent phonons are summarized in Table I. They agree well with the frequencies and linewidths obtained from our Raman scattering measurements on the same sample with sub-band gap excitation, also shown in Table I. Based on the previous Raman studies[7,9] the three phonon modes observed for $\theta = 0°$ and 45° are assigned to the E_g symmetry, whereas the two observed for $\theta = 90°$ are to the B_{1g} and A_{1g} symmetries. The $B_{1g}(\nu_2)$ (at 15.35 THz) and $A_{1g}(\nu_3)$ (at 15.52 THz) modes are nearly degenerate in frequency, and appear as an unresolved asymmetric peak in the Raman spectra with a peak height ratio of ~1 : 4.[9] These six phonon modes comprise all of the bulk Raman-active modes of anatase. Since the Raman intensity and coherent phonon amplitude are proportional to the square of the Raman polarizability and polarizability itself, respectively, we can attribute the coherent response at 15.2 THz to the sum

TABLE I. Frequencies and dephasing rates [half widths at half maximum (HWHM)] of anatase and rutile obtained from transient reflectivity and Raman scattering measurements.

	Transient reflectivity				Raman		
	Frequency		Dephasing		Frequency	HWHM	
Sample	(THz)	(cm^{-1})	(ps^{-1})	(cm^{-1})	(cm^{-1})	(cm^{-1})	Assignment
Anatase	4.36	145	0.72	3.8	145	5	$E_g(\nu_6)$
	5.85	195	>0.3	>1.6	199	2	$E_g(\nu_5)$
	11.83	395	1.57	8.4	396	10	$B_{1g}(\nu_4)$
	15.21	507	2.3	12.4	517	11	$B_{1g}(\nu_2)/A_{1g}(\nu_3)$
	19.09	637	1.6	8.8	638	11	$E_g(\nu_1)$
Rutile	13.3	443	2.5	13	446	19	E_g
	18.2	607	5.6	30	610	22	A_{1g}
					834	19	B_{2g}

of $B_{1g}(\nu_2)$ and $A_{1g}(\nu_3)$ modes with a coherent amplitude ratio of $\sim 1:2$.

We note that the $E_g(\nu_5)$ mode appears as a small dip on the tail of the much larger $E_g(\nu_6)$ peak in the FT spectra [Fig. 2(b)]. This is in marked contrast to the Raman spectra, in which different phonon modes can superimpose in frequency but do not interfere. The FT spectral line shape is determined by the phase relation between the coherent modes over their whole decoherence time, rather than their initial phases at time zero. The initial phase of each coherent phonon mode, which is often related with the generation mechanism, can be determined by fitting the time-domain data with a damped harmonic function. We find that the $E_g(\nu_6)$ mode is a sine function of time (zero amplitude at $t = 0$). Quantitative determination of the initial phase of the $E_g(\nu_5)$ mode is, however, difficult due to its small amplitude. For the high-frequency mode like $E_g(\nu_1)$, experimental ambiguity in defining the exact time zero affects the determination of the initial phase. We therefore examine the generation mechanism by performing an analysis of the dependence of the coherent amplitudes on the polarization angle of the pump light. We base this on the fact that ISRS should depend on the symmetry properties of the phonons (Raman tensors), whereas the TDFS should depend on the dichroism in the optical absorption.

Figures 3(a)–3(c) show plots of the experimentally obtained coherent amplitudes $\Delta R_{eo}(t = 0)/R$ for anatase as we rotate the crystals with respect to the fixed polarizations of pump and probe light. The plots show a complex dependence on the crystal rotation angle, because the measurements are a product of the pump and probe polarization angle dependences. By considering the two dependences separately, however, the observed angular variations are readily interpreted. If coherent phonons are excited via ISRS, the driving force, and hence the coherent phonon amplitude, depends on the direction of the pump electric field through the Raman tensor:[40]

$$F_j(t) = \left(\frac{\partial \chi}{\partial Q}\right)_{jkl} E_k(t) E_l(t). \tag{1}$$

The Raman tensor describes how the Raman scattering cross section for a particular symmetry phonon mode depends on the polarizations of the incident and the scattered field. The symmetry requirements can be analytically expressed by basis function(s) for each phonon symmetry classification.[43]

The dependence of the coherent amplitude on the *pump* polarization angle θ is then given by the angular dependence of the basis function within the crystalline surface plane, $f(\theta)$, as shown in the Supplemental Material.[44] Rotating the *probe* polarization angle also varies how the reflected field amplitude is modified by a given nuclear displacement, because the modulation of the reflectivity ΔR by nuclear displacement ΔQ is mediated by the Raman tensor:[40]

$$\Delta R \simeq \frac{\partial R}{\partial \chi}\frac{\partial \chi}{\partial Q}\Delta Q. \tag{2}$$

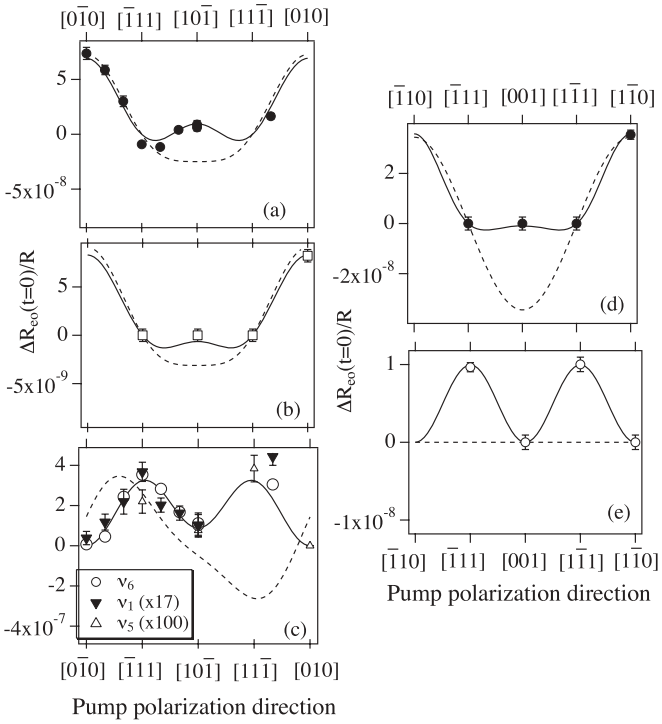

FIG. 3. Polarization dependence of measured (symbols) and calculated (lines) coherent phonon amplitudes detected in the EO configuration: (a) $B_{1g}(\nu_4)$, (b) $B_{1g}(\nu_2)/A_{1g}(\nu_3)$, and (c) E_g symmetry modes of anatase (101), and (d) A_{1g} and (e) E_g symmetry modes of rutile (110). Solid and broken curves represent $G(\theta)$ and $A(\theta)$ functions defined in Eqs. (4) and (5), which assume ISRS and TDFS generation mechanisms, respectively.

In the present EO detection, the probe polarization dependence is given by

$$g(\theta) = f(\theta) - f\left(\theta - \frac{\pi}{2}\right), \tag{3}$$

because we record the difference between the components parallel and perpendicular to the pump polarization angle θ. The overall pump-probe polarization dependence of the ISRS-generation/EO-detection is given by the product

$$G(\theta) = f(\theta)\left[f(\theta) - f\left(\theta - \frac{\pi}{2}\right)\right], \tag{4}$$

which is plotted with solid curves in Figs. 3(a)–3(c) for anatase (101) surface. The calculated $G(\theta)$ reproduces the experimental data well for all the different symmetry phonon modes. This proves that the coherent phonons of anatase are generated via ISRS, as well as confirms the mode symmetry assignments.

If, however, the coherent polar phonons were generated via TDFS, the photoexcited drift-diffusion current along the surface normal direction would give the driving force for the polar phonon mode.[40] The drift-diffusion current would depend on the direction of the pump electric field only through the anisotropy in the optical absorption $\alpha(\theta)$ within the crystalline surface plane.[44] The overall pump-probe polarization dependence of the TDFS-generation/EO-detection would be given by the product

$$A(\theta) = \alpha(\theta)\left[f(\theta) - f\left(\theta - \frac{\pi}{2}\right)\right], \tag{5}$$

which is plotted with broken curves in Figs. 3(a)–3(c). Failure of the calculated $A(\theta)$ in reproducing the experimental data confirms that the TDFS mechanism is negligible in the generation of bulk coherent phonons of anatase excited at the fundamental absorption edge.

We perform similar measurements and analyses on rutile single crystal. The reflectivity change from rutile (110) surface shows a very weak ($\Delta R_{eo}/R \sim 10^{-8}$) modulation at 18.2 THz when the pump light polarization angle θ is 90° from the [001] crystalline axis, and an even weaker modulation at 13.3 THz for $\theta = 45°$ with respect to the axis, as shown in Fig. 4. The two modes are assigned, respectively, to the A_{1g} and E_g phonons based on previous studies.[5,45] The frequencies and dephasing rates, listed in Table I, agree with our Raman measurements on the same sample. The coherent phonons of rutile, especially the E_g mode, dephase faster than those of anatase due to a large cubic anharmonicity associated with three-phonon processes.[6] The other two Raman active modes of rutile, the B_{1g} and B_{2g} modes at 4.29 and 24.8 THz, are not observed as the reflectivity modulation, presumably because of their smaller Raman scattering cross sections compared to the A_{1g} and E_g modes.[5] The B_{2g} mode is detected as a very weak peak in the Raman spectra from the same sample (Table I).

Figures 3(d) and 3(e) plot the experimentally obtained pump-probe polarization dependence of coherent amplitudes for rutile (110) surface, together with the calculations assuming ISRS and TDFS generations. The polarization dependence calculated after Eq. (4) [solid curves in Figs. 3(d) and 3(e)] reproduces the experimental data well, whereas that after Eq. (5) (broken curves in the same figure) does not. The results indicate that the observed coherent phonons are generated via

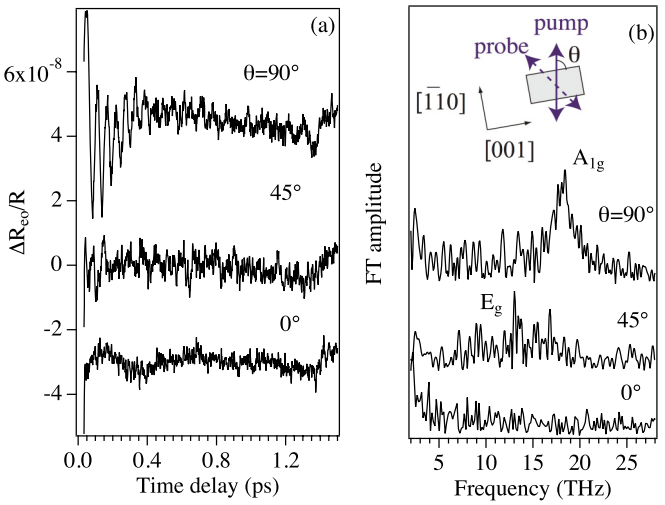

FIG. 4. (Color online) (a) Oscillatory parts of anisotropic reflectivity changes and (b) their FT spectra from the (110) surface of rutile TiO_2 at different pump polarization angles θ. Traces are offset for clarity. Inset in (b) shows the polarization of pump and probe beams with respect to the crystal. The sample is rotated while the polarizations of pump and probe beams are fixed in vertical and 45° from vertical orientations.

ISRS also for rutile single crystal, as well as confirm the mode symmetry assignments. Our observation is consistent with the previous reflectivity study on a rutile (110) surface using nonresonant (620 nm), but intense (8 mJ/cm^2) optical pulses.[39] There, only the A_{1g} phonon was observed as a large-amplitude ($\Delta R/R \lesssim 10^{-4}$) modulation of reflectivity, and the generation was attributed to the ISRS mechanism based on its sine-like initial phase. By contrast, the same study observed a surface phonon mode at 13.2 THz by means of the SSHG detection, and related it to the bulk E_u mode based on its polarization dependence and its cosine-like initial phase indicating TDFS generation.[39] Though the frequency of our bulk E_g mode (13.3 THz) is close to that of the surface mode, in the present study we find no evidence for the TDFS generation, as is expected for a nonpolar E_g-symmetry mode. We thereby conclude that the two studies have indeed observed different-symmetry phonon modes with different detection methods.

The Raman scattering contributing to the ISRS generation process can in general be either nonresonant or resonant. We test for the resonance effect by varying the pump-probe wavelength between 397 and 387 nm (3.12 and 3.20 eV). With the laser bandwidth of ~ 20 nm, this wavelength range coincides with the sub-band-gap absorption (Urbach) tail of anatase[18] and above-band-gap absorption of rutile;[15,18] the dichroic absorption of anatase increases by an order of magnitude, whereas that of rutile is stronger but exhibits less variation. For rutile, a resonant Raman study reported a sharp enhancement in the A_{1g} phonon scattering efficiency at 3.03 eV due to an exciton double resonance, but little enhancement in the E_g phonon due to a single resonance.[24] A hyper-Raman scattering study observed monotonic increase in the scattering efficiency of the allowed (Raman-inactive) phonons with increasing two-photon energy.[25] In the present time-resolved measurements at room temperature, however, we find no significant wavelength dependence in coherent

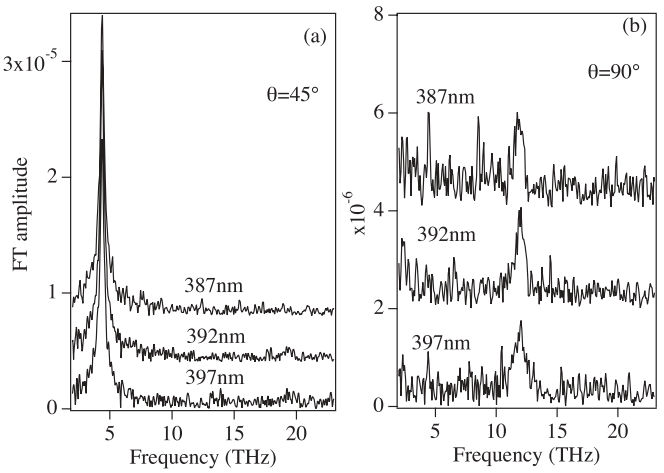

FIG. 5. FT spectra of anisotropic reflectivity changes from anatase (101) for $\theta = 45^\circ$ (a) and 90° (b) pumped and probed at different wavelengths. Traces are offset for clarity.

phonons for either anatase (Fig. 5) or rutile (not shown). The observation, together with the very small amplitude in the reflectivity modulation, indicates nonresonant ISRS generation of the coherent phonons in both polymorphs. The absence of the resonance enhancement is attributed to the indirect and symmetry-forbidden direct band gaps that occur in this wavelength region. [21,22,24,25] Contribution by the excitonic resonance is negligible in the present study, because the laser wavelength is shifted from the very narrow double resonance for rutile,[24] and because the creation of self-trapped excitons is too slow compared with the phonon oscillation periods for anatase.[31]

The resonance enhancement of ISRS, as well as the TDFS generation of the polar phonons, is more likely to occur at the symmetry-allowed direct band gaps of rutile and anatase at 3.6–4.2 and 3.7–3.9 eV.[22] Further investigations under the resonant excitation at the direct band gaps should reveal the nature of the carrier-lattice coupling, especially the role of the anisotropic exciton wave functions predicted for both rutile and anatase.[22] For TiO_2 nanocrystals, the electron-phonon dynamics are expected to be modified significantly by photoexcitation and trapping via surface defects and dopants. For dye-sensitized TiO_2 surfaces, where the resonance is defined by the chromophore absorption spectrum, the ultrafast interfacial charge injection into the semiconductor could give a driving force for phonon dynamics that is qualitatively different from nonsensitized surfaces.[39,41] The present study on the bulk phonons of nonsensitized TiO_2 single crystals gives a baseline for further experimental and theoretical investigations on the bulk and nanocrystalline TiO_2 samples, as well as sensitized TiO_2 interfaces.

IV. CONCLUSION

Raman-active bulk phonon modes were observed as coherent modulations of reflectivity of anatase and rutile TiO_2 single crystals under photoexcitation near the fundamental absorption edge with NUV light. The dependence of the coherent phonon amplitudes on the pump and probe polarization angles was related quantitatively to the angular dependence of the Raman tensor components within the crystalline surface plane. We thus demonstrated that the Raman scattering is responsible as the generation and detection mechanisms for all the bulk phonon modes observed for anatase and rutile single crystals. The coherent oscillations showed no significant dependence on the photon energy between 3.12 and 3.20 eV, suggesting that the resonance enhancement in the Raman generation process is negligible near the absorption edge corresponding to the indirect band gaps. The knowledge obtained in the present study will contribute to understanding the ultrafast electron-phonon dynamics in the bulk, nanocrystal, and adsorbate-modified surfaces.

ACKNOWLEDGMENT

This research was partially supported by NSF CHE-1213189 grant.

*ishioka.kunie@nims.go.jp

[1] A. Fujishima, X. Zhang, and D. A. Tryk, Surf. Sci. Rep. **63**, 515 (2008).
[2] A. Hagfeldt and M. Grätzel, Acc. Chem. Res. **33**, 269 (2000).
[3] A. Cowan, J. Tang, W. Leng, J. Durrant, and D. Klug, J. Phys. Chem. C **114**, 4208 (2010).
[4] J. Zhang, M. J. Li, Z. C. Feng, J. Chen, and C. Li, J. Phys. Chem. B **110**, 927 (2006).
[5] S. Porto, P. Fleury, and T. Damen, Phys. Rev. **154**, 522 (1967).
[6] T. Lan, X. Tang, and B. Fultz, Phys. Rev. B **85**, 094305 (2012).
[7] T. Ohsaka, F. Izumi, and Y. Fujiki, J. Raman Spectroscopy **7**, 321 (1978).
[8] K. Lagarec and S. Desgreniers, Solid State Commun. **94**, 519 (1995).
[9] M. Giarola, A. Sanson, F. Monti, G. Mariotto, M. Bettinelli, A. Speghini, and G. Salviulo, Phys. Rev. B **81**, 174305 (2010).
[10] N. Park, G. Schlichthorl, J. van de Lagemaat, H. Cheong, A. Mascarenhas, and A. Frank, J. Phys. Chem. B **103**, 3308 (1999).
[11] V. Swamy, A. Kuznetsov, L. S. Dubrovinsky, R. A. Caruso, D. G. Shchukin, and B. C. Muddle, Phys. Rev. B **71**, 184302 (2005); V. Swamy, *ibid.* **77**, 195414 (2008).
[12] G. R. Hearne, J. Zhao, A. M. Dawe, V. Pischedda, M. Maaza, M. K. Nieuwoudt, P. Kibasomba, O. Nemraoui, J. D. Comins, and M. J. Witcomb, Phys. Rev. B **70**, 134102 (2004).
[13] W. Zhang, Y. He, M. Zhang, Z. Yin, and Q. Chen, J. Phys. D **33**, 912 (2000).
[14] M. Cardona and G. Harbeke, Phys. Rev. **137**, A1467 (1965).
[15] J. Pascual, J. Camassel, and H. Mathieu, Phys. Rev. B **18**, 5606 (1978).
[16] A. Amtout and R. Leonelli, Phys. Rev. B **51**, 6842 (1995).
[17] H. Tang, K. Prasad, R. Sanjines, P. Schmid, and F. Levy, J. Appl. Phys. **75**, 2042 (1994).

[18]H. Tang, F. Levy, H. Berger, and P. E. Schmid, Phys. Rev. B **52**, 7771 (1995).
[19]L. Kavan, M. Grätzel, S. Gilbert, C. Klemenz, and H. Scheel, J. Am. Chem. Soc. **118**, 6716 (1996).
[20]S.-D. Mo and W. Y. Ching, Phys. Rev. B **51**, 13023 (1995).
[21]C. Persson and A. da Silva, Appl. Phys. Lett. **86**, 231912 (2005).
[22]L. Chiodo, J. M. Garcia-Lastra, A. Iacomino, S. Ossicini, J. Zhao, H. Petek, and A. Rubio, Phys. Rev. B **82**, 045207 (2010).
[23]W. Kang and M. S. Hybertsen, Phys. Rev. B **82**, 085203 (2010).
[24]A. Amtout and R. Leonelli, Phys. Rev. B **46**, 15550 (1992).
[25]K. Watanabe and K. Inoue, Phys. Rev. B **41**, 7957 (1990); K. Watanabe, K. Inoue, and F. Minami, *ibid.* **46**, 2024 (1992).
[26]E. Yagi, R. R. Hasiguti, and M. Aono, Phys. Rev. B **54**, 7945 (1996).
[27]E. Hendry, F. Wang, J. Shan, T. F. Heinz, and M. Bonn, Phys. Rev. B **69**, 081101 (2004).
[28]N. A. Deskins and M. Dupuis, Phy. Rev. B **75**, 195212 (2007).
[29]L. Forro, O. Chauvet, D. Emin, L. Zuppiroli, H. Berger, and F. Levy, J. Appl. Phys. **75**, 633 (1994).
[30]M. Watanabe and T. Hayashi, J. Lumin. **112**, 88 (2005).
[31]T. Sekiya, M. Tasaki, K. Wakabayashi, and S. Kurita, J. Lumin. **108**, 69 (2004); K. Wakabayashi, Y. Yamaguchi, T. Sekiya, and S. Kurita, *ibid.* **112**, 50 (2005).
[32]V. P. Zhukov and E. V. Chulkov, J. Phys.: Condens. Matter **22**, 435802 (2010); V. P. Zhukov, V. G. Tyuterev, and E. V. Chulkov, *ibid.* **24**, 405802 (2012).
[33]D. Colombo, K. Roussel, J. Saeh, D. Skinner, J. Cavaleri, and R. Bowman, Chem. Phys. Lett. **232**, 207 (1995).
[34]K. Iwata, T. Takaya, H. Hamaguchi, A. Yamakata, T. Ishibashi, H. Onishi, and H. Kuroda, J. Phys. Chem. B **108**, 20233 (2004).
[35]M. Salmi, N. Tkachenko, R. Lamminmaki, S. Karvinen, V. Vehmanen, and H. Lemmetyinen, J. Photochem. Photobio. A **175**, 8 (2005).
[36]Y. Tamaki, K. Hara, R. Katoh, M. Tachiya, and A. Furube, J. Phys. Chem. C **113**, 11741 (2009).
[37]K. Yamanaka and T. Morikawa, J. Phys. Chem. C **116**, 1286 (2012).
[38]L. Dhar, J. Rogers, and K. Nelson, Chem. Rev. **94**, 157 (1994).
[39]T. Nomoto, A. Sasahara, and H. Onishi, J. Chem. Phys. **131**, 084703 (2009).
[40]M. Först and T. Dekorsy, in *Coherent Vibrational Dynamics*, edited by S. D. Silvestri, G. Cerullo, and G. Lanzani (CRC, Boca Raton, 2007), p. 129.
[41]W. A. Tisdale, K. J. Williams, B. A. Timp, D. J. Norris, E. S. Aydil, and X.-Y. Zhu, Science **328**, 1543 (2010).
[42]E. Portuondo-Campa, A. Tortschanoff, F. van Mourik, and M. Chergui, J. Chem. Phys. **128**, 244718 (2008).
[43]G. Burns, *Introduction to Group Theory with Applications* (Academic Press, New York, 1977).
[44]See Supplemental Material at http://link.aps.org/supplemental/10.1103/PhysRevB.86.205201 for the derivation of $G(\theta)$ and $A(\theta)$ for the different-symmetry phonon modes in anatase and rutile.
[45]C. Lee, P. Ghosez, and X. Gonze, Phys. Rev. B **50**, 13379 (1994).